

**NASA
Technical
Paper
2869**

December 1988

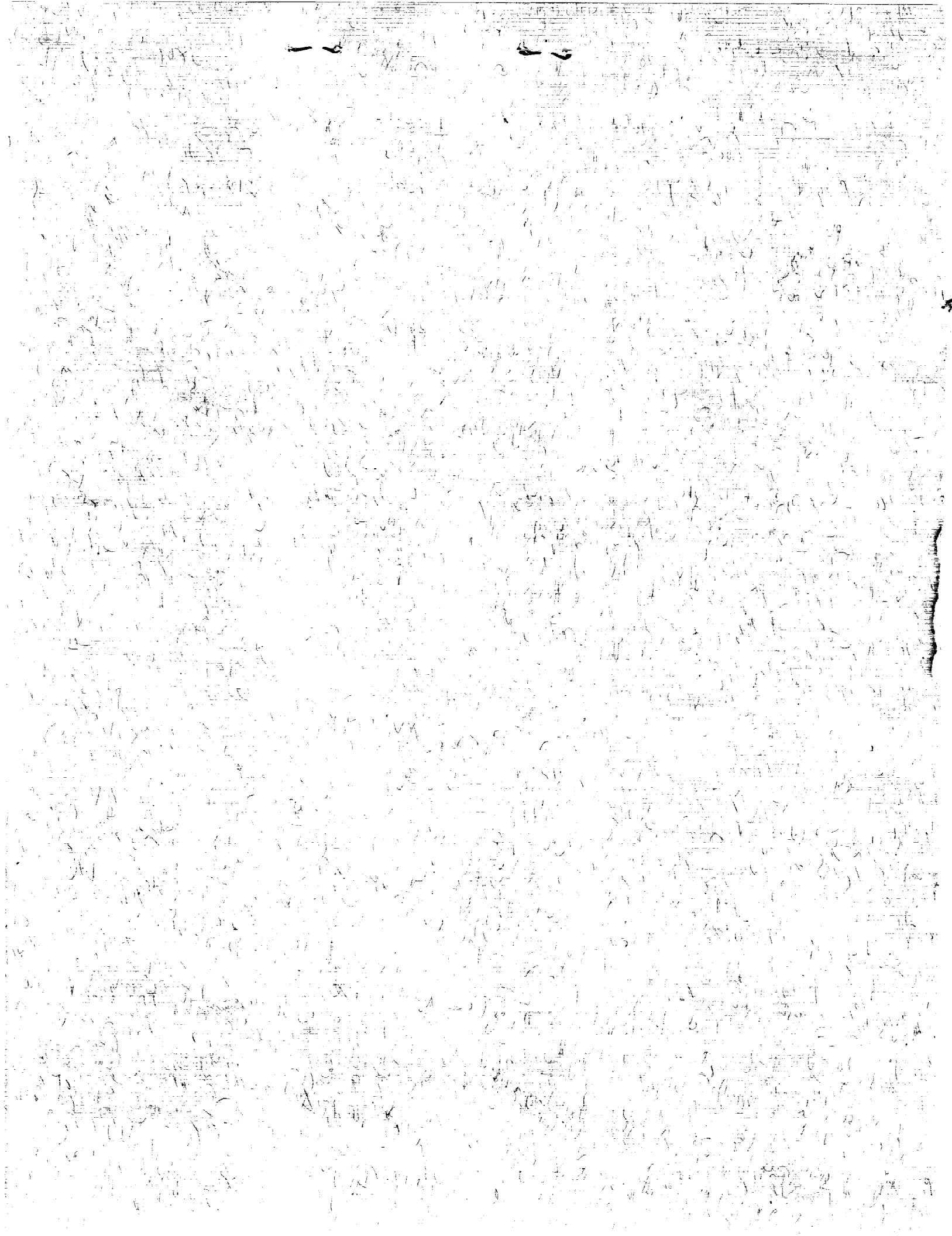
Solar-Flare Shielding With Regolith at a Lunar-Base Site

John E. Nealy,
John W. Wilson, and
Lawrence W. Townsend

(NASA-TP-2869) SOLAR-FLARE SHIELDING WITH
REGOLITH AT A LUNAR-BASE SITE (NASA) 21 p
CSCL 03B

889-14210

H1/93 Unclas
0168969



**NASA
Technical
Paper
2869**

1988

Solar-Flare Shielding With Regolith at a Lunar-Base Site

John E. Nealy,
John W. Wilson, and
Lawrence W. Townsend
*Langley Research Center
Hampton, Virginia*

NASA

National Aeronautics
and Space Administration

Scientific and Technical
Information Division

Introduction

As more specific extended-duration lunar missions are envisioned, environmental parameters such as high-energy, charged-particle radiation from solar flares and galactic cosmic rays become very important. Large solar flares can release great quantities of high-energy nucleons for time periods as long as several days. Also, very high-energy galactic cosmic rays bombard the Moon steadily from sources outside the solar system. Unlike on Earth, lunar inhabitants will not have the protective cover of an atmosphere or magnetic-field regions as a shield against these radiations; therefore, their health and safety will be endangered.

In this study, an analysis is made of solar-flare events and of a probable means for protection of lunar inhabitants. For relatively short-duration missions (2 to 3 months), the most important radiation hazards are the very high fluxes of energetic solar-flare protons that are produced. Solar flares may also contain X rays and gamma rays, electrons, neutrons, and some heavier charged particles as well as the protons. However, examination of previous observations of large flare radiation fluxes indicates that if the shielding against the high-energy protons is effective, the absorbed doses from the other solar radiations are probably not significant. (See chapter V of ref. 1.)

The purpose for this study was twofold: (1) To demonstrate the capabilities of using an off-line data base generated with a comprehensive radiation transport code to predict dose patterns within various configurations, and (2) To provide initial estimates of dose levels caused by large solar proton events for candidate lunar-base modules shielded with lunar regolith. The magnitudes of doses computed in the present study are compared with the recommended dose limits established for volunteer astronauts. (See ref. 2.) One of the more important radiation doses for humans is for a 5-cm depth in the body. In this study, the dose at 5-cm depth is considered representative of the dose to the blood-forming organs (BFO dose). The specified maximum levels at this 5-cm depth are 25 rem/month and 50 rem/year. Therefore, the shielding for protection from solar flares should limit doses to substantially less than 25 rem for a single event. Physical radiation dose (rad) is determined by the amount of energy deposited per unit mass of material. To account for the differences in damage produced in biological matter due to various types of radiation, the physical dose is multiplied by an energy-dependent quality factor to obtain the dose equivalent (rem). In this study, the quality factor used in conversion of physical dose to dose equivalent

is that recommended in reference 3; this factor is appropriate for evaluation of long-term effects resulting from exposure.

Description of Computational Procedure

The transport of nucleons through layered shielding material is modeled by the Langley Baryon Transport computer code BRYNTRN. (See ref. 4.) This code uses an algorithm which provides solutions of the one-dimensional Boltzmann transport equation and is a deterministic, as opposed to statistical, model. In the one-dimensional, or straight-ahead, approximation for energetic particles, this integro-differential equation may be written as

$$\begin{aligned} & [\partial/\partial x - \partial/\partial E S_i(E) + \sigma_i(E)] \Phi_i(x, E) \\ & = \sum_j \int_E^\infty \sigma_{ij}(E, E') \Phi_j(x, E') dE' \end{aligned}$$

where Φ_i is the flux of type i nucleons (protons or neutrons) at position x in the shield layer with energy E in the range dE . The σ_i values are the total nuclear absorption cross sections and represent attenuation of the propagating beam. The $\sigma_{ij}(E, E')$ values are the differential nuclear interaction cross sections and represent processes in which type i particles of energy $E' (> E)$ interact with type j (target) particles to produce type i particles of energy E and, therefore, to augment the beam at that energy. While the σ_{ij} values impose most of the mathematical complexity in solving the transport equation, their contributions are crucial to the particle flux solutions and are consequently handled with considerable detail in the code. The $S(E)$ term (stopping power or linear energy transfer (LET)) represents the practically continuous loss of energy due to interaction of energetic charged particles with atomic orbital electrons. The stopping power for protons used in the code is based on the Bethe formula. A detailed discussion of the solution methodology and nuclear cross-section data base used may be found in reference 4.

Three of the largest flares observed in the last half century have been chosen for analysis of radiation-dose levels produced. The time-integrated (flare-duration) proton fluence spectra for these three events (ref. 5) are shown in figure 1, where the number of protons per unit area in the vicinity of the Earth's orbit with energy greater than a given value is plotted. The flare of August 1972 produced the greatest total number of protons but had fewer protons than the other two events for energies greater than approximately 150 MeV. The February 1956 event produced approximately one-tenth as many

protons as the 1972 flare, but delivered far more protons than both other flares of 200 MeV or greater. The November 1960 flare spectrum exhibits characteristics intermediate to the others with regard to both low- and high-energy particles. Energy spectra and dose predictions are presented for these three solar flares, and variations in shielding effectiveness because of the different energy distributions are predicted. The flare data shown in figure 1 were also used in a recent study which examined the shielding properties of aluminum and water. (See ref. 6.)

The transport code may be adapted for an arbitrary number of shield-material constituent atoms. In the case of a lunar-soil model, five of the more abundant elements occurring in regolith samples were chosen: O, Si, Mg, Al, and Fe. This selection is based on sample concentrations given in a previous lunar base study. (See ref. 7.) Considerable variability was reported in return sample compositions, and the inclusion of Mg instead of Ca in the 5-element soil model is somewhat questionable since many sample returns showed slightly more Ca than Mg. For the present study, a series of lengthy transport calculations was used first with Mg in the soil model. A comparison calculation with Ca substituted for Mg showed insignificant effects on the computed doses, and it was deemed unnecessary to perform a parametric study of soil models. Consequently, for this study, the lunar soil composition (normalized to measured abundances of SiO₂, Al₂O₃, FeO, and MgO) is considered to have the elemental percentages given in table I:

Table I. Lunar-Soil Model

Element	Normalized composition, percent atoms/g
O	61.5
Si	19.3
Al	7.5
Fe	6.1
Mg	5.5

The soil mass density was assumed to be 1.5 g/cm³, based on the density range of 0.8 to 2.15 g/cm³ reported in reference 7.

The transport code is set up to give results corresponding to a monodirectional beam of particles at normal incidence on a slab of given thickness. In making computations related to a specific geometry (e.g., a cylinder or sphere rather than a slab), the transport code was used for a series of thicknesses of lunar regolith (slab geometry), and the output was placed in accessible permanent data files. The

stored output included proton and neutron energy spectra as functions of target thickness. Also, for each specified slab thickness, predicted doses in tissue as the result of the transport of the emergent nucleons through 20 cm of simulated tissue material are stored. Tissue dose due to contributions by protons, neutrons, and high-energy heavy-ion (HZE) recoil processes are recorded for twenty 1-cm increments. The recoil processes are caused by heavy nuclei being displaced by nucleon impact. (Tissue material for this study is simulated by water.)

Examples of data stored from this procedure are illustrated graphically in figures 2 through 4, where the proton and neutron fluxes are shown for four depths in the lunar material for the three flares in the energy range between 10 and 1000 MeV. The differences in energy distribution arising as a result of the initial proton spectra are exhibited, and particularly noteworthy is the insensitivity to shield thickness (penetrability) of neutrons having energies in excess of 100 MeV. In other words, neutron attenuation decreases markedly with increasing energy. A simple proton range calculation for material of this density using the Bethe formula demonstrates that the preponderance of these particles are secondaries, which again illustrates the importance of the nuclear interaction processes. For example, the range of penetration of 100-MeV protons in material of density 1.5 g/cm³ is approximately 7 cm (see chapter 3 of ref. 8); nevertheless, the flare calculations show that protons of energies lower than 100 MeV are predicted to be in relative abundance for regolith slabs of thicknesses considerably larger than 7 cm. The types of data exhibited in figures 2 through 4 are later accessed by the geometry algorithm applicable to a specific configuration.

Dose Predictions for Slab Layers

General shielding properties of lunar regolith for large-flare proton fluxes normally incident on slab layers are shown in figure 5. Here, the resultant rem dose at 5-cm depth in tissue (BFO dose) has been computed as a function of regolith slab thickness for the three flares under consideration. The consequences of the different energy characteristics of the flares are evident. The 1972 flare, with large fluxes of low-energy protons, is at or near the lethal dose (\approx 500 rem at 5-cm tissue depth) with no shielding, whereas for 50 cm of regolith shield, the computed dose is well below 1 rem, which would be considered nonhazardous. For the February 1956 event, the unshielded dose level, while predicted to be near the established annual BFO dose limit, is nowhere near lethal; however, the abundance of high-energy

particles for this flare results in a much more penetrating flux. Even with 50 cm of shielding, the predicted BFO dose for this event is well above 10 rem (definitely of significance to an astronaut on a long-duration mission who may be accumulating dose from other sources). Results for the November 1960 event are between the two extremes.

The dose variation in tissue is given in figure 6 for the particle fluxes emergent from 10-, 25-, and 50-cm layers of regolith. The dose variation is most dramatic for the 1972 event because of its high-flux/low-energy characteristics. The dose at the 5-cm depth is less than half the skin dose (or surface dose) and is less than one-tenth of the skin-dose value at 20 cm. This result demonstrates that significant differences can exist between skin or eye dose and the BFO dose and that caution must be used in extrapolating between dose at depth and skin dose. Figure 6 also shows that 10-cm regolith shielding is inadequate for such large proton flares; the 5-cm-depth dose exceeds the 30-day limit of 25 rem. These results also indicate that there should be more interest in shield layers of 50 cm or more to reduce the BFO dose below the 25-rem limit. Figure 6 also shows that the differences between skin dose and 5- to 20-cm tissue depth dose are not as severe for slab layers of 50 cm.

Results for Specific Configurations

The data base generated with the transport code has been applied to determine radiation fields inside simple geometric structures that represent lunar habitation modules shielded by regolith layers. These radiation fields have been used to predict corresponding dose equivalents. For each geometry (cylinders and spheres); distances in the shield material are determined by the particular wall thickness traversed on a straight-line path from a given point outside the structure to a specified target point within the enclosure. The computational procedure used established the internal target point as the origin of a spherical coordinate system. The shield (or wall) thickness encountered by a ray directed from the origin is then related to the usual azimuth and zenith direction angles. (See fig. 7(a).) Increments of 5° were used to encompass the entire range of directions (72 azimuth angles between 0° and 360° , and 36 zenith angles between 0° and 180°). The computational method can be adapted to more complex configurations by using multiple sectional analytic surfaces or surface grid data. Spherical and cylindrical configurations are chosen for this study because of their applicability to proposed lunar habitation structures. (See ref. 9.)

To evaluate the dose at a particular target point, the radiation from all directions must be determined. Figure 7(b) illustrates the dose variation with the direction of incoming radiation for a target point at the geometric center of a half-buried cylinder with constant shielding thickness on the walls above the surface. Because of the approximate logarithmic dependence of radiation flux on the target material thickness traversed, the directional patterns can be highly variable. The nature of the directional patterns also changes markedly with target point position, particularly for the cylindrical configuration. A similar representation is shown in figure 8 for a half-buried shielded sphere with target points displaced from the center by a distance equal to 80 percent of the radius and for zenith angles of 45° (above ground level) and 135° (below ground level). The pattern asymmetries are obvious. The illustrations of figures 7 and 8 are intended here only as qualitative depictions of one part of the computational procedure. Quantitative directional data are not routinely analyzed. However, representations of this type are valuable for assessing geometrical effects. In practice, the directional-field data are simply multiplied by the solid-angle increment appropriate to the directional grid and integrated to obtain the total radiation dose at a target point.

Isodose contour plots have been generated for a cylindrical volume that is assumed to be placed on the lunar surface. The shield is assumed to be in contact with the cylinder walls, to be of constant thickness on top of the cylinder, and to be increasing in thickness below the cylinder axis. (See fig. 9.) The particular dimensions chosen for the cylinder correspond approximately to the Freedom space-station module: length 12.2 m in length and 4.6 m in diameter. The ends of the cylinder are assumed to have shield layers of thickness equal to that prescribed for the overhead thickness. For an overhead regolith thickness of 50 cm, the dose variation for the November 1960 solar flare inside the module is shown in figure 10 for horizontal planes 1 m above the centerline, at the centerline, and 1 m below the centerline. The general dose level shows little change for heights at and above the center plane; there are decreases at the lower level. The smaller radiation levels below the center plane are the result of closer proximity to the lunar surface (here taken to be opaque to all radiations), and larger shield thicknesses in this lower plane. Also noteworthy are the field maxima occurring at about two-thirds the distance between the center and end walls; these maxima can indicate positions to avoid during flare activity. Figure 11 shows corresponding results for the same flare and configuration for an overhead regolith thickness of 100 cm.

The qualitative variations are similar, but the overall dose levels have been reduced approximately one order of magnitude.

The isodose map for a half-buried sphere with a regolith shield thickness of 50 cm above the lunar surface is shown in figure 12 for the 1960 flare. The field maximum dose occurs above the center point at approximately one-third the radius. The diameter of the sphere is 15.2 m. The isodose map for the same sphere and shield configuration for the 1956 event is shown in figure 12(b). The 5-cm BFO dose levels are generally higher as a result of the abundance of high-energy protons. Also, the maximum dose occurs at a position nearer the top of the sphere. As a synopsis, table II gives the computed doses for 50- and 100-cm regolith shielding at the midpoints of the cylinder on the lunar surface and the half-buried sphere, for all three solar-flare events. The corresponding normal-incidence slab doses are included.

Table II. 5-cm Depth Dose Comparisons for Three Large Flares

Flare date	Shield thickness, cm	Predicted dose, rem		
		Cylinder (center)	Sphere (center)	Slab
1956	50	7.48	7.04	13.30
	100	2.70	2.94	5.55
1960	50	1.60	1.90	3.59
	100	.16	.23	.43
1972	50	0.25	0.30	0.56
	100	.03	.04	.07

For the cylindrical and spherical configurations, the dose is reduced by approximately 50 percent because of the shield effect of the underlying surface. As the isodose maps indicate, however, the dose level may vary considerably from point to point within an enclosure.

Analysis of Results

The purpose of this study has been to provide estimates of radiation doses from large solar flares that will be incurred by a person inside a structure on the lunar surface with a thick regolith shield. For the half-buried spherical module with a 50-cm regolith top shield, the maximum interior dose is slightly in excess of 9 rem for the 1956 solar flare. The two following important factors modify these predictions, and both tend to reduce the dose.

1. No consideration has been given to the shielding effects of wall materials, the supporting structure,

or the placement of equipment in and around the module.

2. The effects of human geometry have been neglected, in that the 5-cm BFO doses are predicted in terms of radiation received at the center of a 5-cm sphere of human tissue.

Also, it is unreasonable to assume that a crew member inside the module remains in the location of maximum dose throughout the flare event.

It must also be emphasized that other contributions to radiation dose exist at the lunar surface. Although flares may constitute the major threat for relatively short-duration missions (especially during maximum solar cycle conditions), longer stays (4 to 6 months or more) will require consideration of the galactic cosmic ray (GCR) dose. The problems of protection from the very high-energy galactic cosmic rays are different from those associated with solar flares in many respects. The GCR fluxes are low relative to solar flares, but are approximately constant with time. The GCR energies can be extremely high ($\gg 1$ GeV), and a dominant dose component is provided by the HZE contribution. Previous calculations for aluminum shields indicate that relatively large thicknesses (≈ 10 cm) are required to restrict the rem dose to an acceptable annual level. (See ref. 10.) Accurate predictions for GCR shielding are requisite to long-duration missions.

The use of lunar soil as a shielding material is attractive in that shielding materials need not be transported to the lunar base. In all likelihood, regolith will be utilized, not only as a radiation-shielding medium, but also as a thermal-control insulating material. This latter aspect has been investigated recently in some detail (ref. 11); a 2-m regolith thickness was found adequate to control heat gain and loss within cylindrical modules. It is, of course, desirable to minimize the amount of lunar soil that must be handled to provide necessary shielding and thermal control, since expenditure of time and energy in the lunar environment will be limited.

Concluding Remarks

The results obtained from studying the doses caused by three large flares indicate that shielding is essential. While 50 cm of regolith thickness may provide adequate flare protection, larger thicknesses may be more desirable. The importance of shield geometry is exemplified in isodose maps for cylindrical and spherical habitation modules. Such analyses may be of consequence in the interior arrangement of the complete module. For example, location of sleeping quarters, placement of equipment, and distribution of water supply may be

impacted by predicted dose distributions. Also, the nucleon transport code BRYNTRN is ideally suited for determination of shielding requirements dictated by the high-energy, charged-particle, space-radiation environment.

NASA Langley Research Center
Hampton, VA 23665-5225
November 17, 1988

References

1. Švestka, Zdeněk: *Solar Flares*. D. Reidel Publ. Co., Inc., c.1976.
2. *Space Station Program Definition and Requirements, Section 3: Space Station Systems Requirements*. SSP 30000, Section 3, Revision F, Space Station Program Off., May 6, 1988.
3. *Recommendations of the International Commission on Radiological Protection*. ICRP Publ. 26, Pergamon Press, Jan. 17, 1977.
4. Wilson, John W.; Townsend, Lawrence W.; Chun, Sang Y.; Buck, Warren W.; Khan, Ferdous; and Cucinotta, Frank: *BRYNTRN: A Baryon Transport Computer Code—Computation Procedures and Data Base*. NASA TM-4037, 1988.
5. Wilson, John W.: Environmental Geophysics and SPS Shielding. *Workshop on the Radiation Environment of the Satellite Power System*, Walter Schimmerling and Stanley B. Curtis, eds., LBL-8581 (Contract W-7405-ENG-48), Univ. of California, Sept. 15, 1978, pp. 33-116.
6. Townsend, Lawrence W.; Nealy, John E.; and Wilson, John W.: *Preliminary Estimates of Radiation Exposures for Manned Interplanetary Missions From Anomalously Large Solar Flare Events*. NASA TM-100620, 1988.
7. Dalton, Charles; and Hohmann, Edward, eds.: *Conceptual Design of a Lunar Colony*. NASA CR-129164, 1972.
8. Profio, A. Edward: *Radiation Shielding and Dosimetry*. John Wiley & Sons, Inc., c.1979.
9. Alred, J.; Bufkin, A.; Graf, J.; Kennedy, K.; Patterson, J.; Petro, A.; Roberts, M.; Stecklein, J.; and Sturm, J.: *Development of a Lunar Outpost: Year 2000-2005. Lunar Bases & Space Activities in the 21st Century*, NASA, AIAA, Lunar & Planetary Inst., American Geophysical Union, American Nuclear Soc., American Soc. of Civil Engineers, Space Studies Inst., and National Space Soc., 1988, Paper No. LBS-88-240.
10. Wilson, John W.; Townsend, Lawrence W.; and Atwell, William: *Preliminary Estimates of Galactic Cosmic Ray Exposures for Manned Interplanetary Missions*. NASA TM-100519, 1987.
11. Simonsen, Lisa C.; DeBarro, Marc J.; Farmer, Jeffery T.; and Thomas, Carolyn C.: *Conceptual Design of a Lunar Base Thermal Control System. Lunar Bases & Space Activities in the 21st Century*, NASA, AIAA, Lunar & Planetary Inst., American Geophysical Union, American Nuclear Soc., American Soc. of Civil Engineers, Space Studies Inst., and National Space Soc., 1988, Paper No. LBS-88-225.

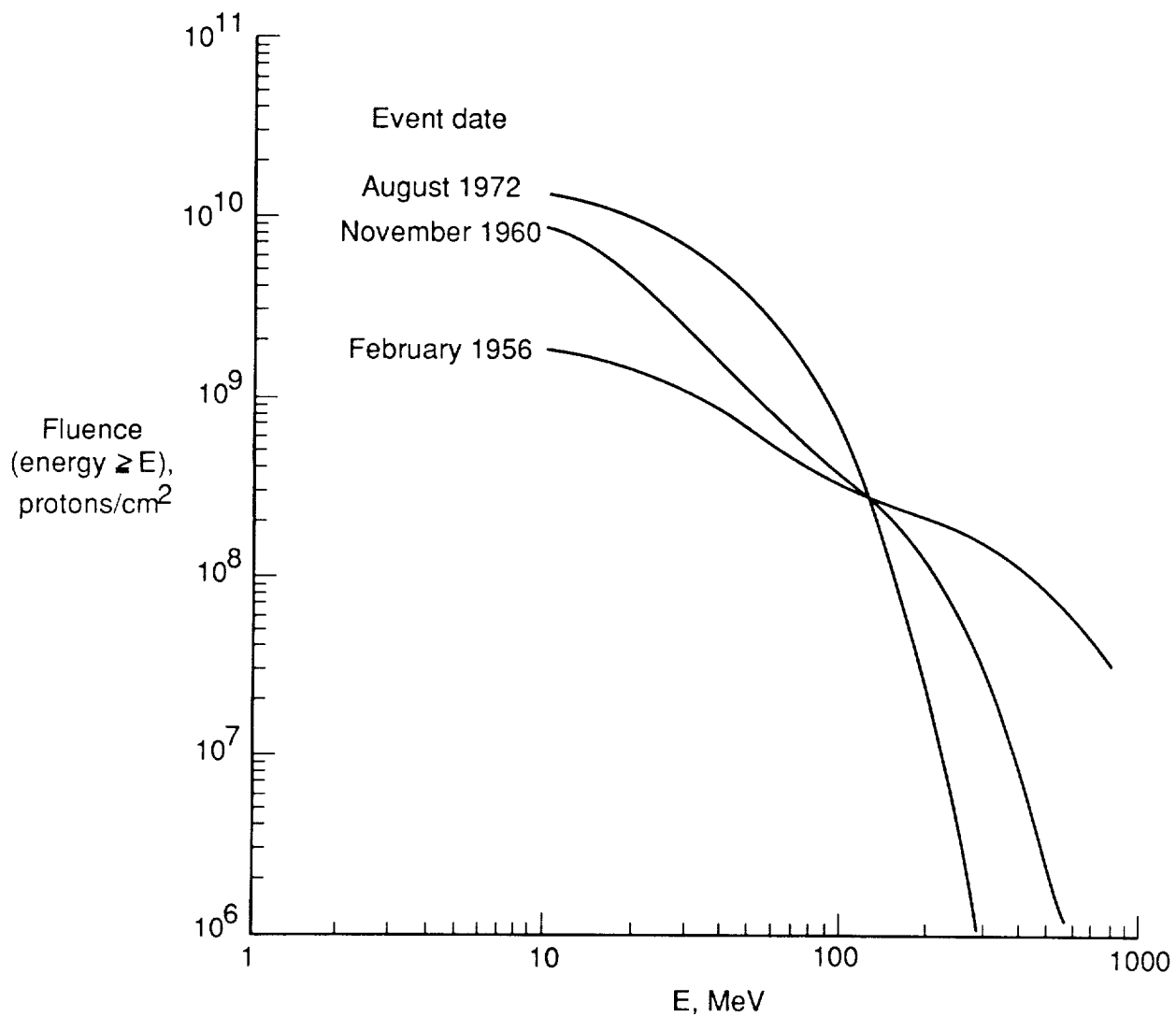


Figure 1. Time-integrated proton flux spectra for three anomalously large solar proton events. (From ref. 6.)

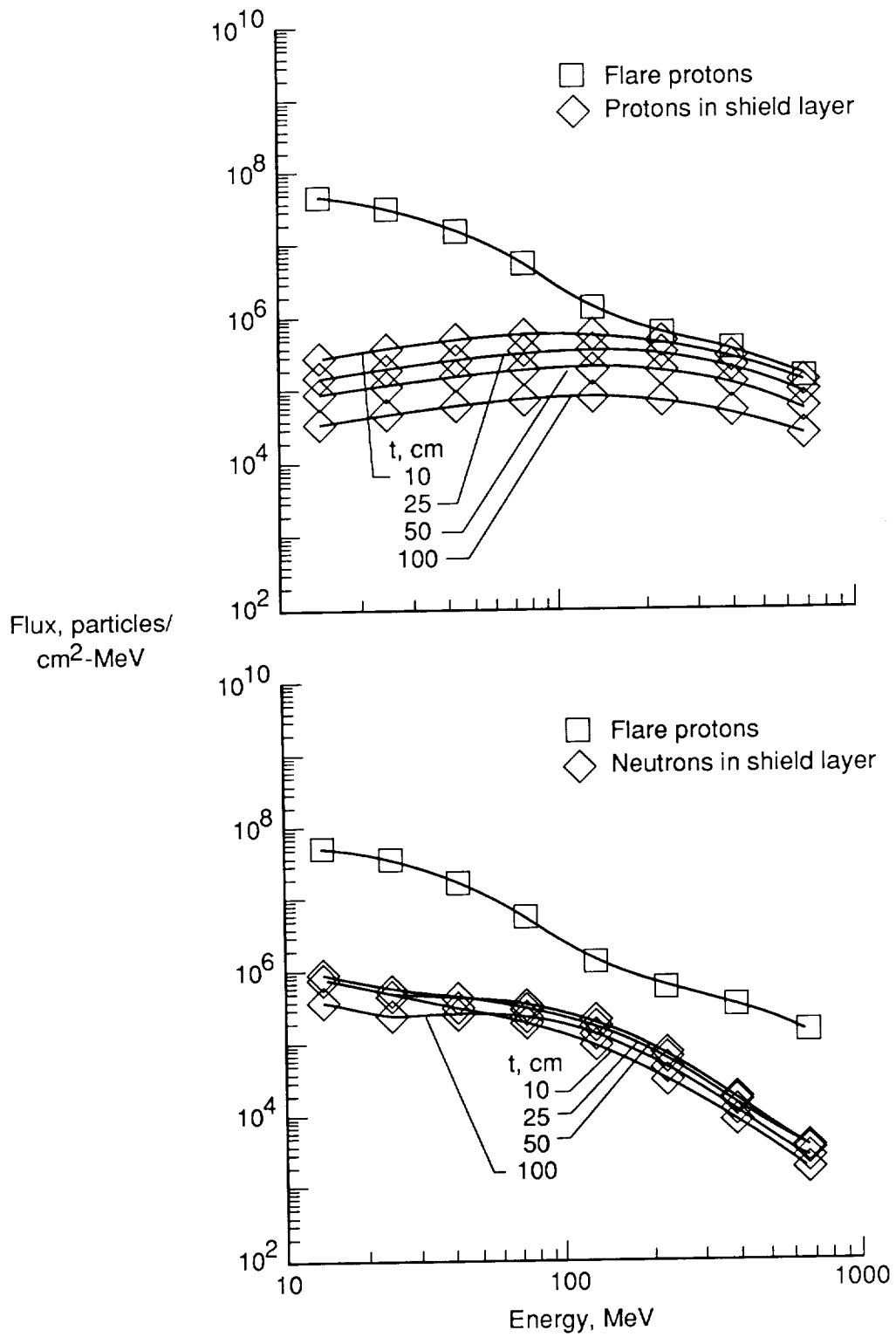


Figure 2. Calculated nucleon flux variation with energy for indicated values *t* of regolith thickness for proton event of February 1956.

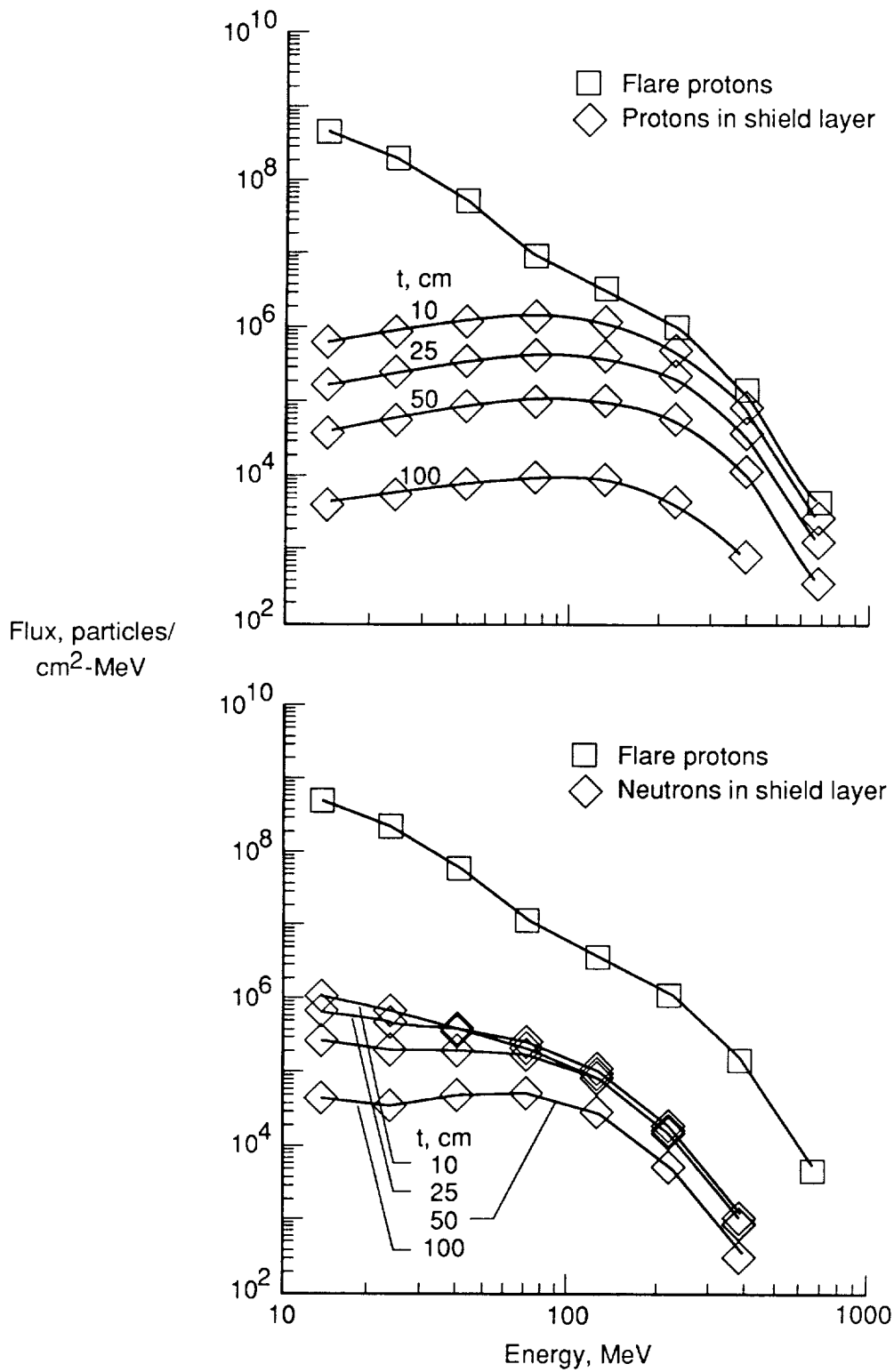


Figure 3. Calculated nucleon flux variation with energy for indicated values *t* of regolith thickness for proton event of November 1960.

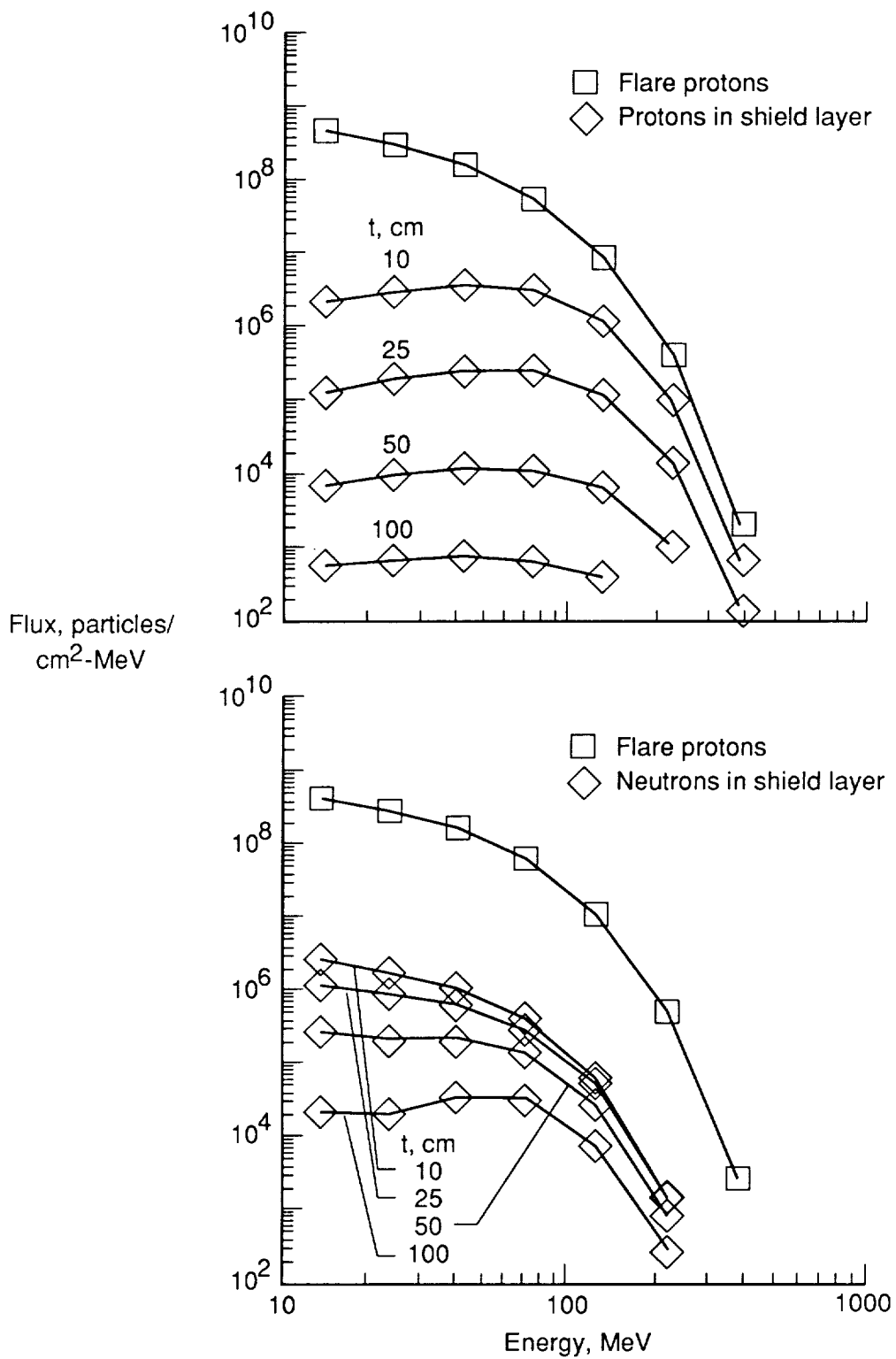


Figure 4. Calculated nucleon flux variation with energy for indicated values t of regolith thickness for proton event of August 1972.

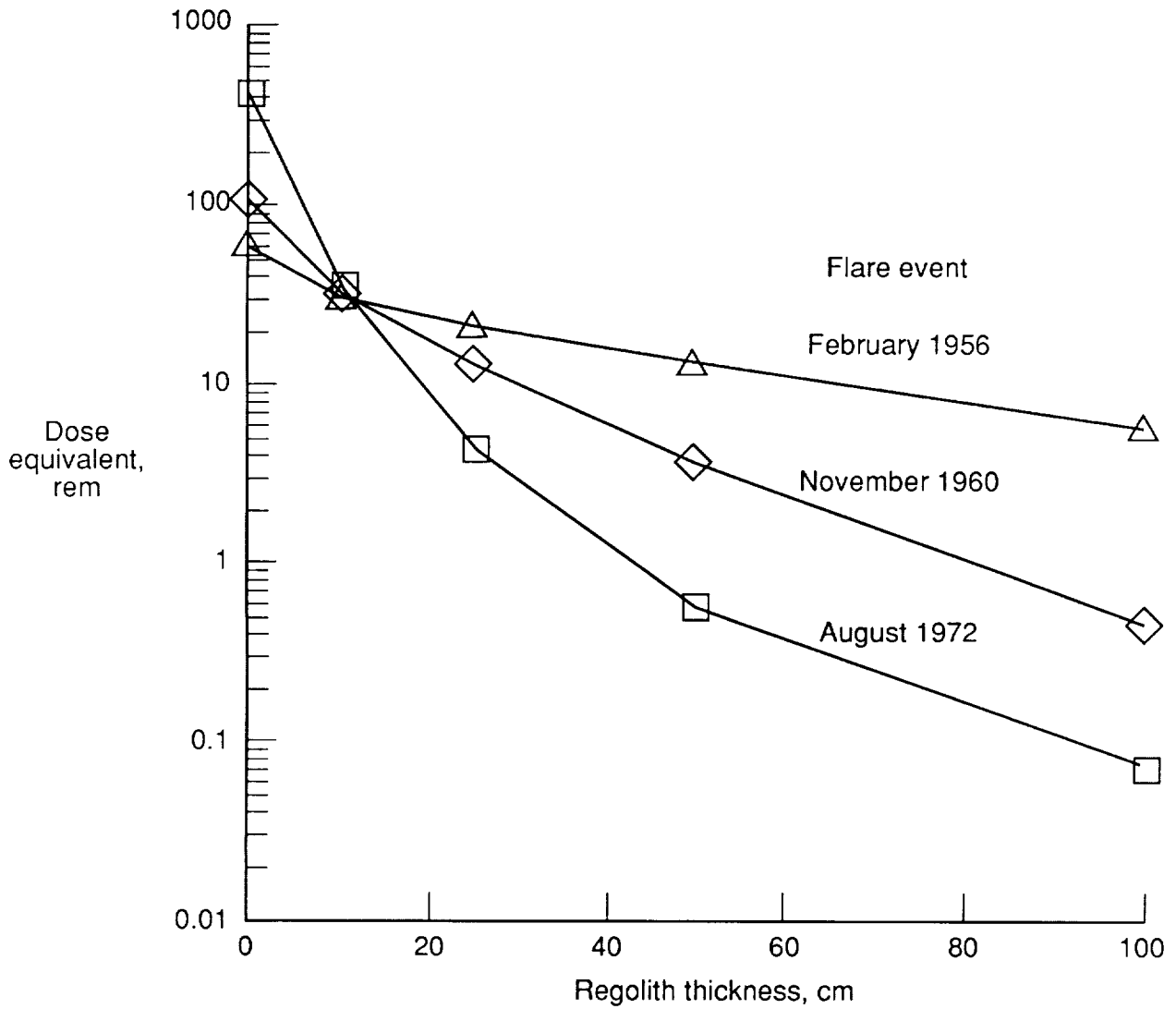


Figure 5. Predicted 5-cm-tissue dose equivalents for slab thicknesses between 0 and 100 cm in simulated lunar regolith.

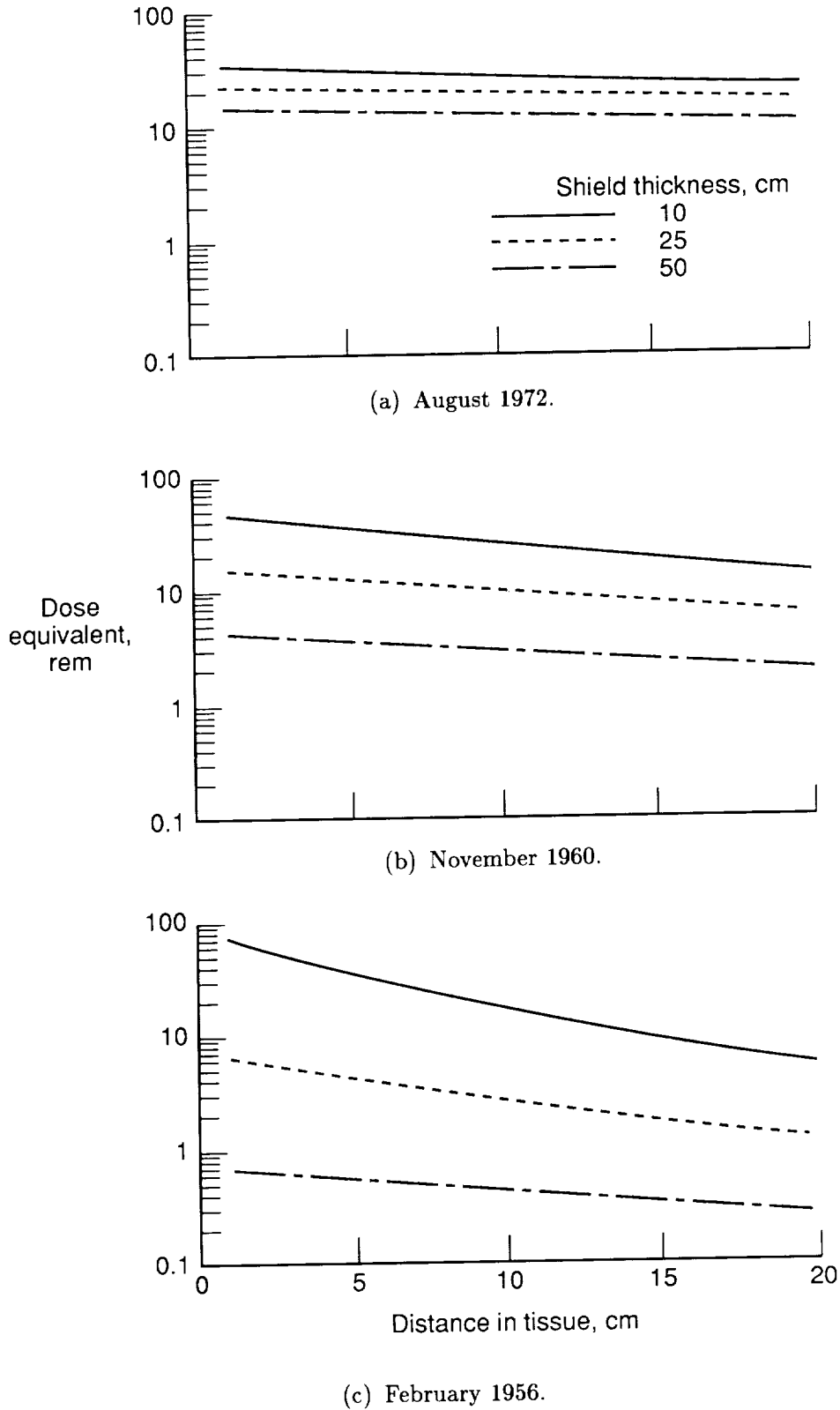
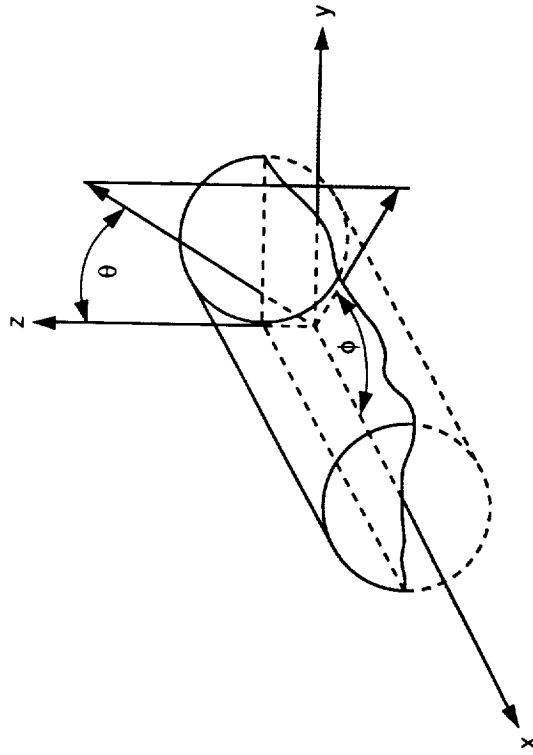
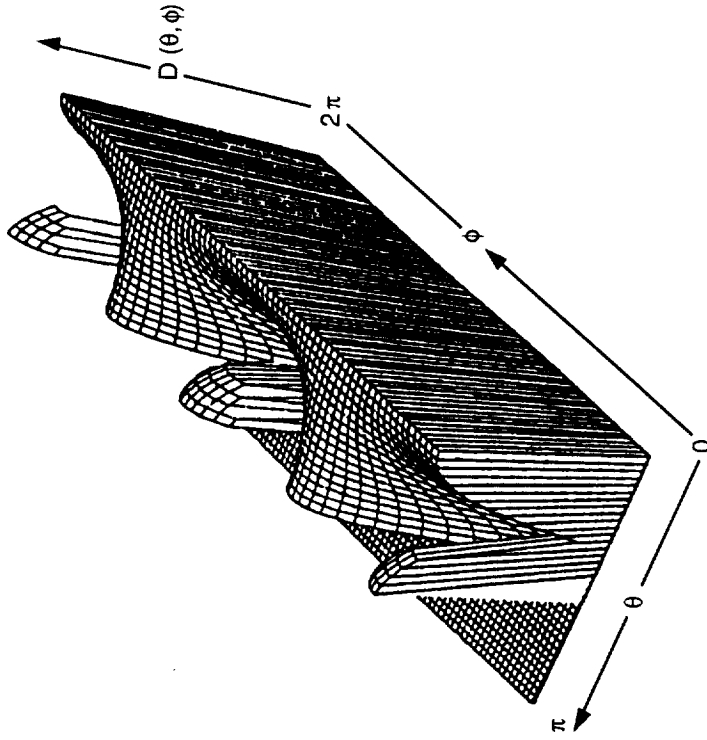


Figure 6. Predicted dose-equivalent variation with depth of tissue for three regolith shield thicknesses and three large proton flares.

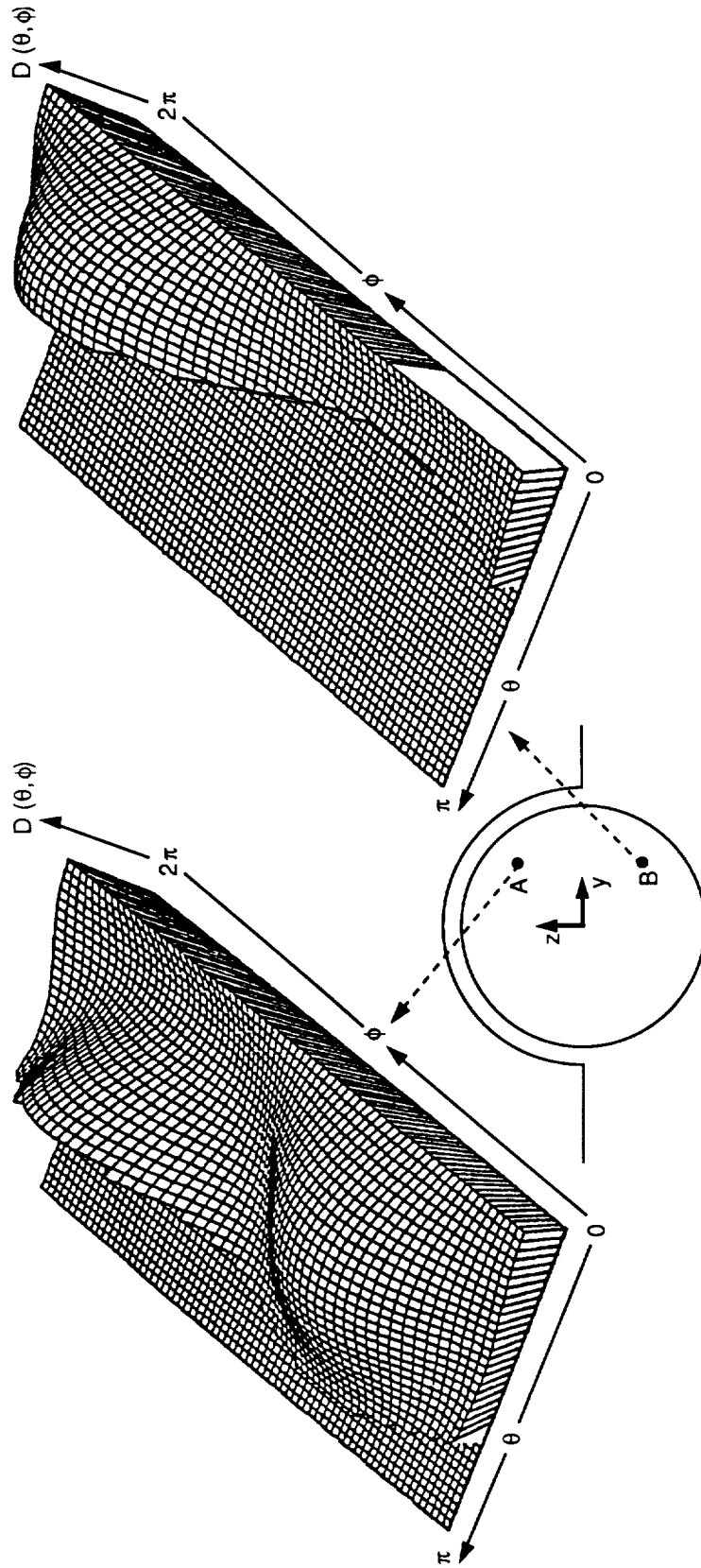


(a) Target-point coordinate system.



(b) Resultant variation of directional dose $D(\theta, \phi)$ as a function of azimuth ϕ and zenith θ angles.

Figure 7. Simulated lunar habitation module (half-buried cylinder).



(a) Upper quadrant.

(b) Lower quadrant below surface level.

Figure 8. Sample directional dose patterns for regolith-shielded, half-buried sphere for target points A and B in the y - z plane as indicated in schematic. D = Directional dose; θ = Zenith angle; ϕ = Azimuth angle.

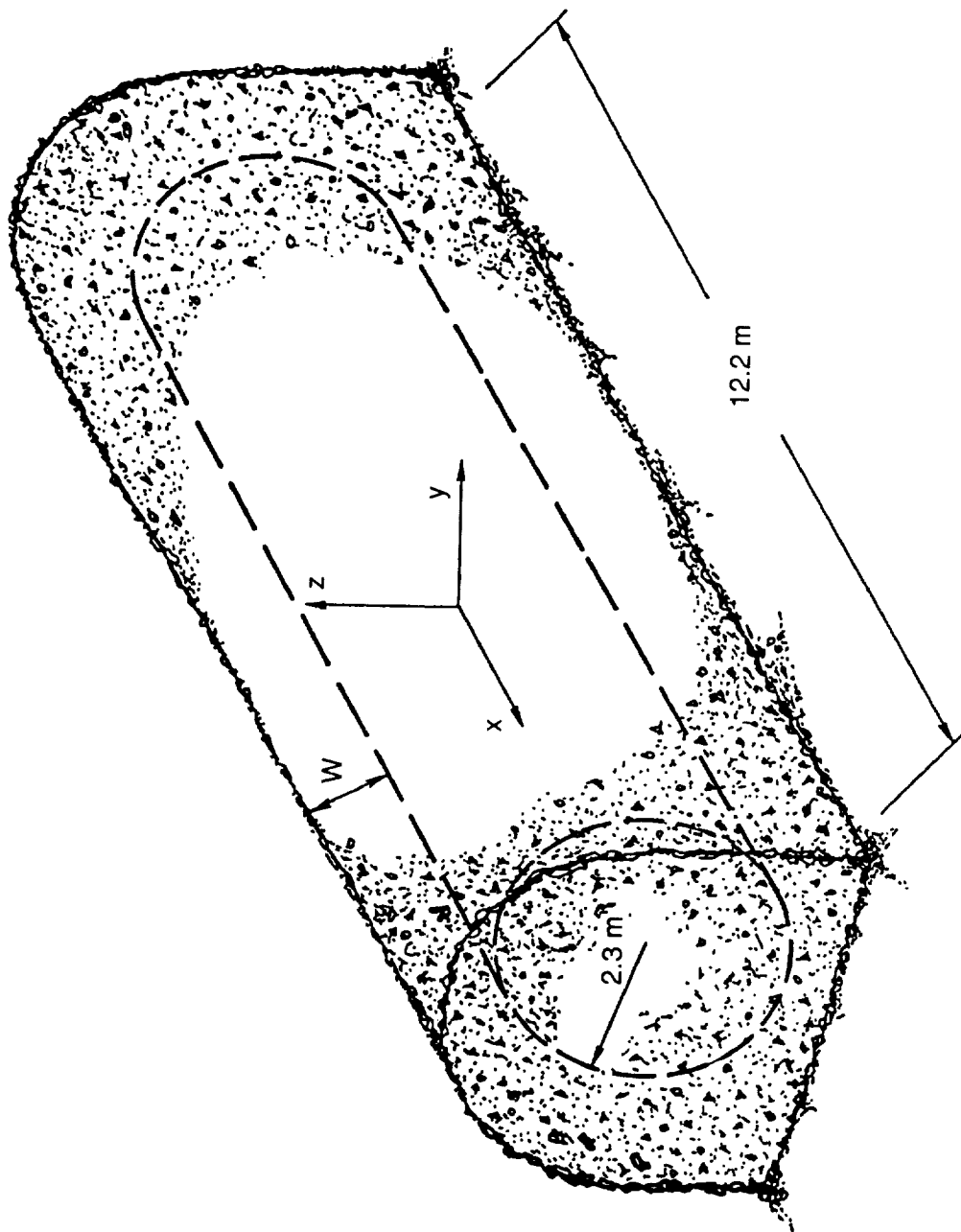
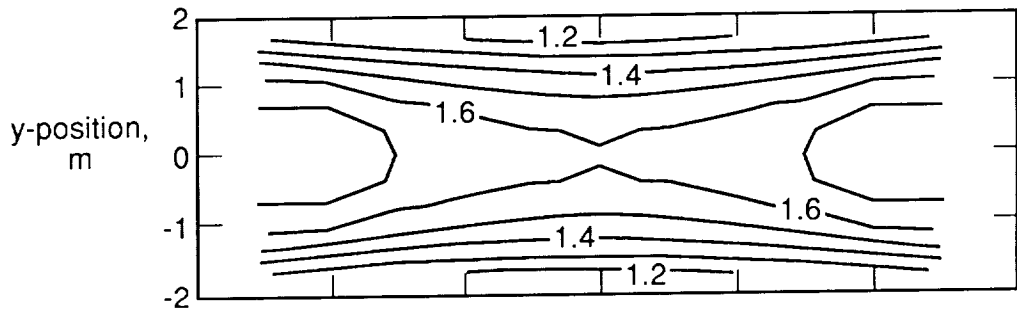
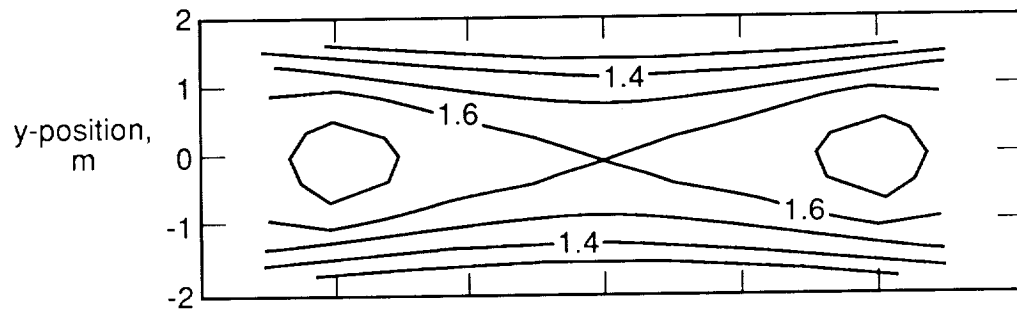


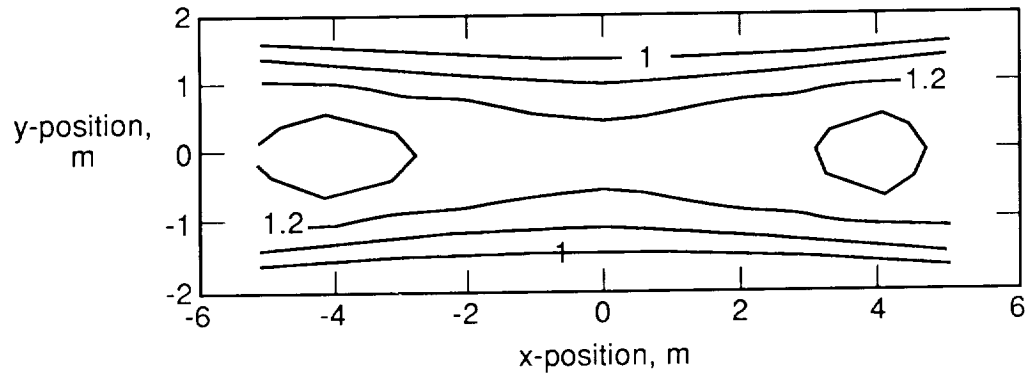
Figure 9. Depiction of regolith shield around cylindrical module on lunar surface. (Configuration used for dose map calculations of figs. 10 and 11.) W = Overhead regolith thickness.



(a) 1 m above center plane.

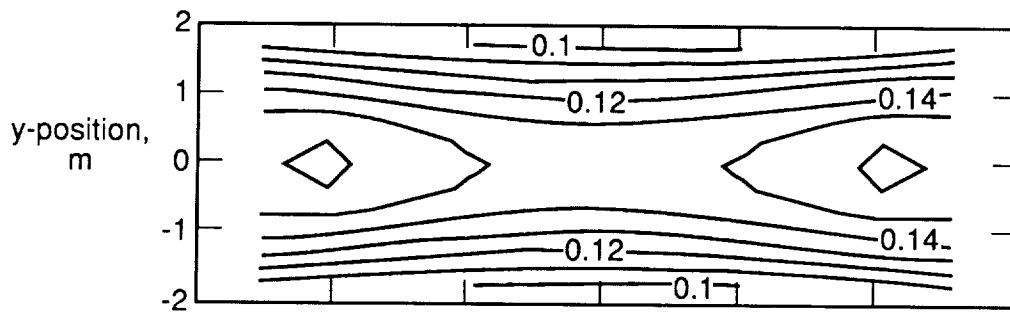


(b) At center plane.

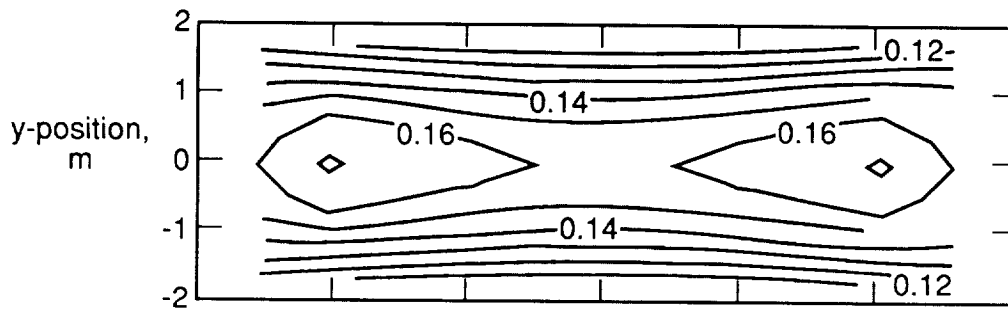


(c) 1 m below center plane.

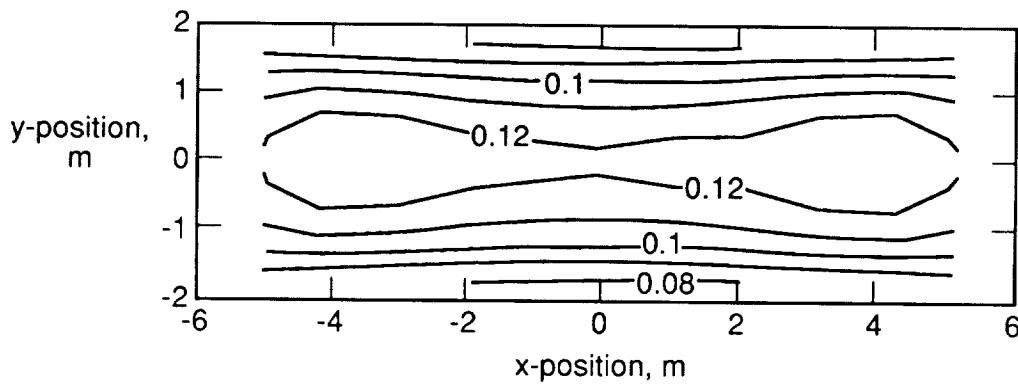
Figure 10. Isodose maps for cylindrical module of figure 9 for top shield thickness of 50 cm for flare of November 1960. Doses are in rem for 5-cm tissue depth (BFO dose); Contour interval = 0.1 rem.



(a) 1 m above center plane.

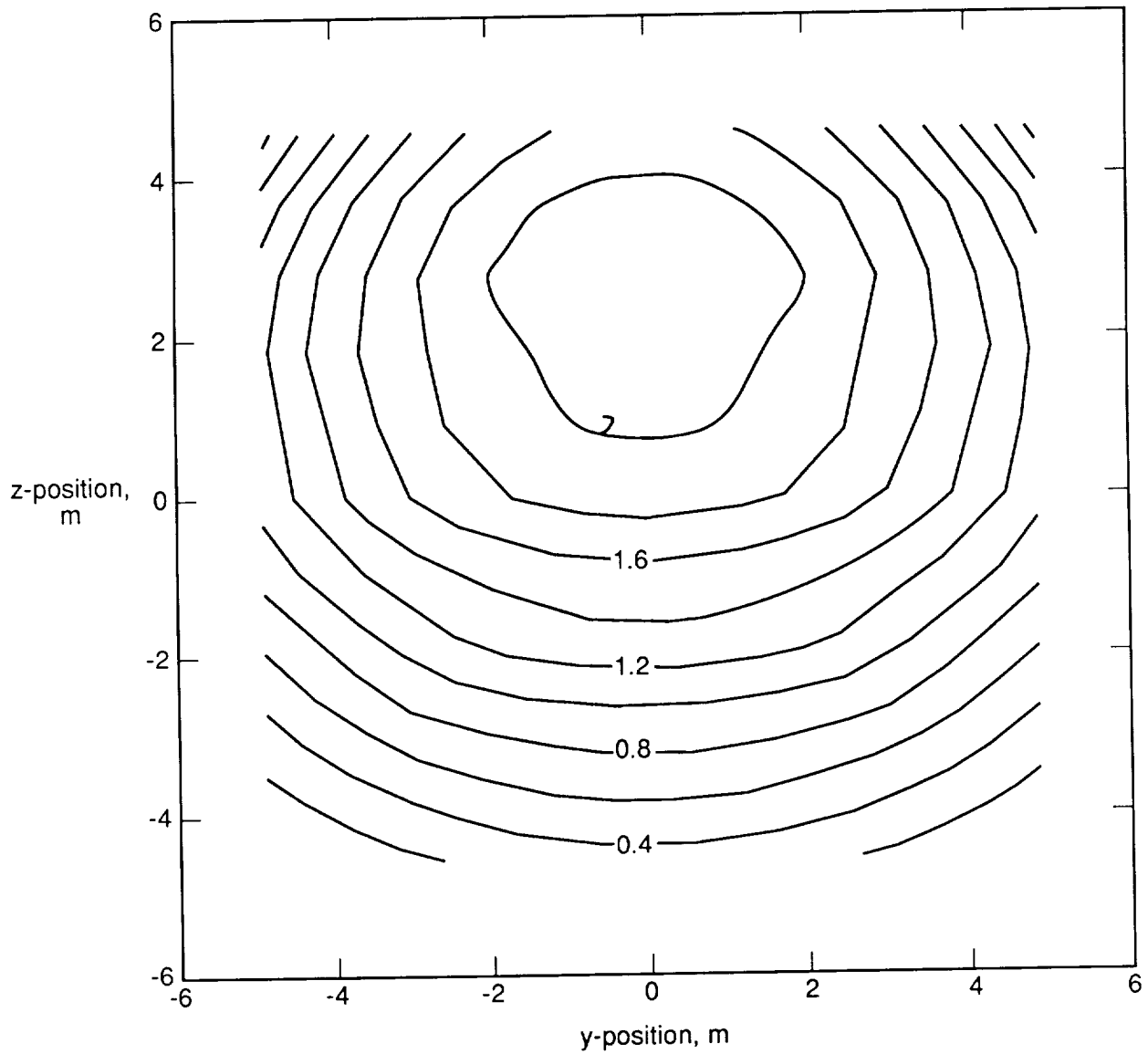


(b) At center plane.



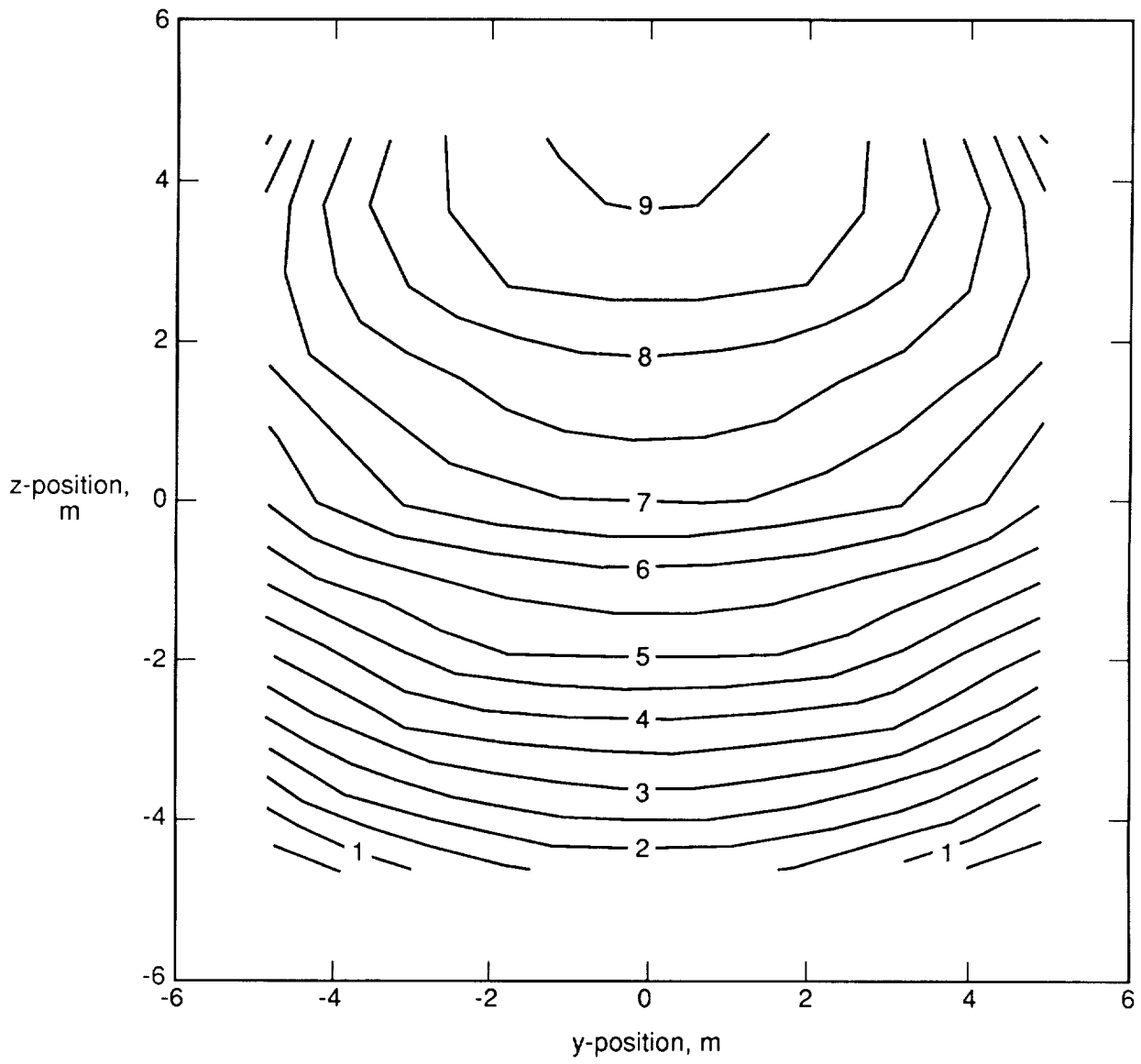
(c) 1 m below center plane.

Figure 11. Isodose maps for cylindrical module of figure 9 for top shield thickness of 100 cm for flare of November 1960. Doses are in rem for 5-cm tissue depth (BFO dose); Contour interval = 0.01 rem.



(a) November 1960 flare.

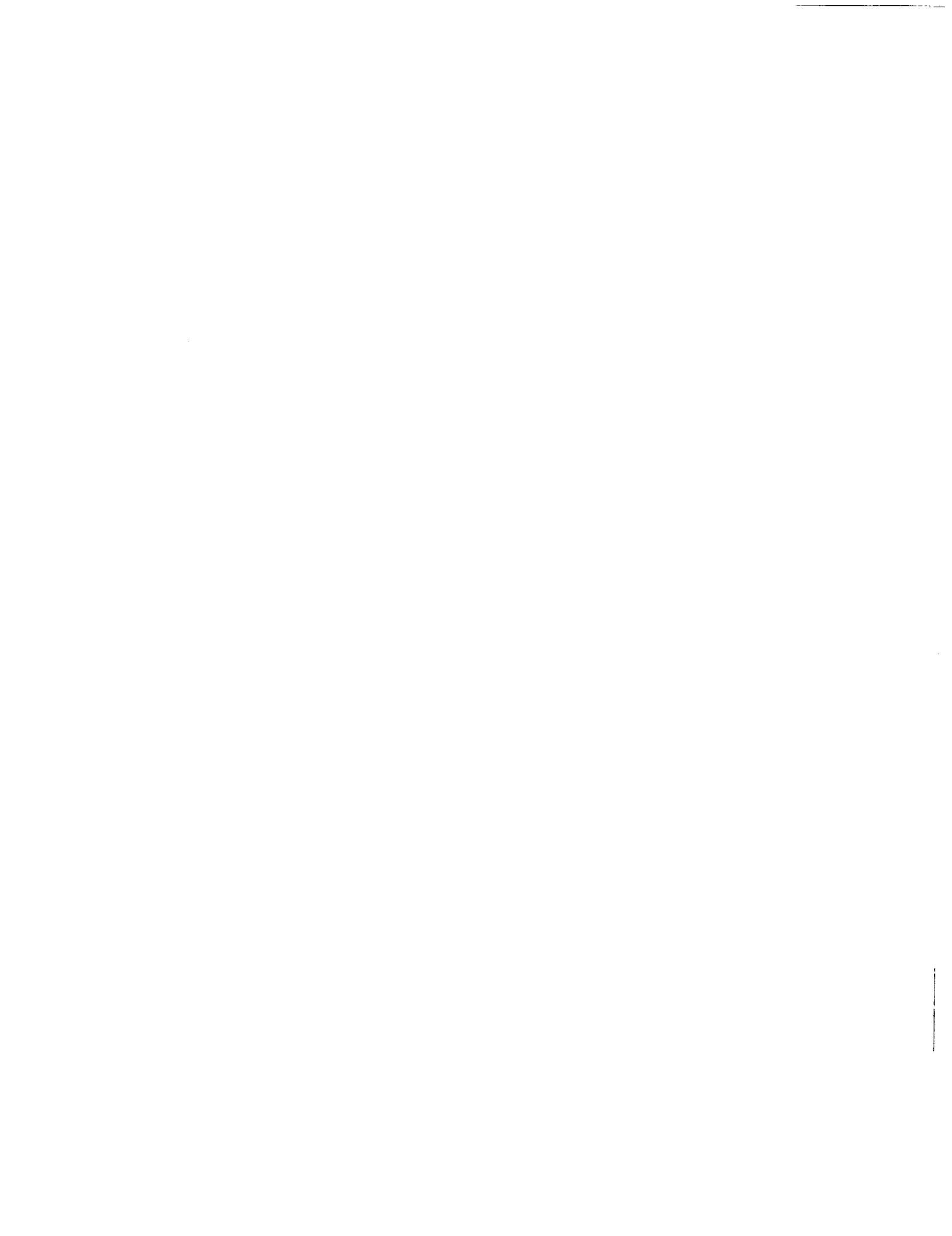
Figure 12. Portion of isodose map for half-buried sphere of 15.24-m diameter with top shield thickness of 50 cm. Doses are in rem at 5-cm tissue depth (BFO dose.)



(b) February 1956 flare.

Figure 12. Concluded.

|

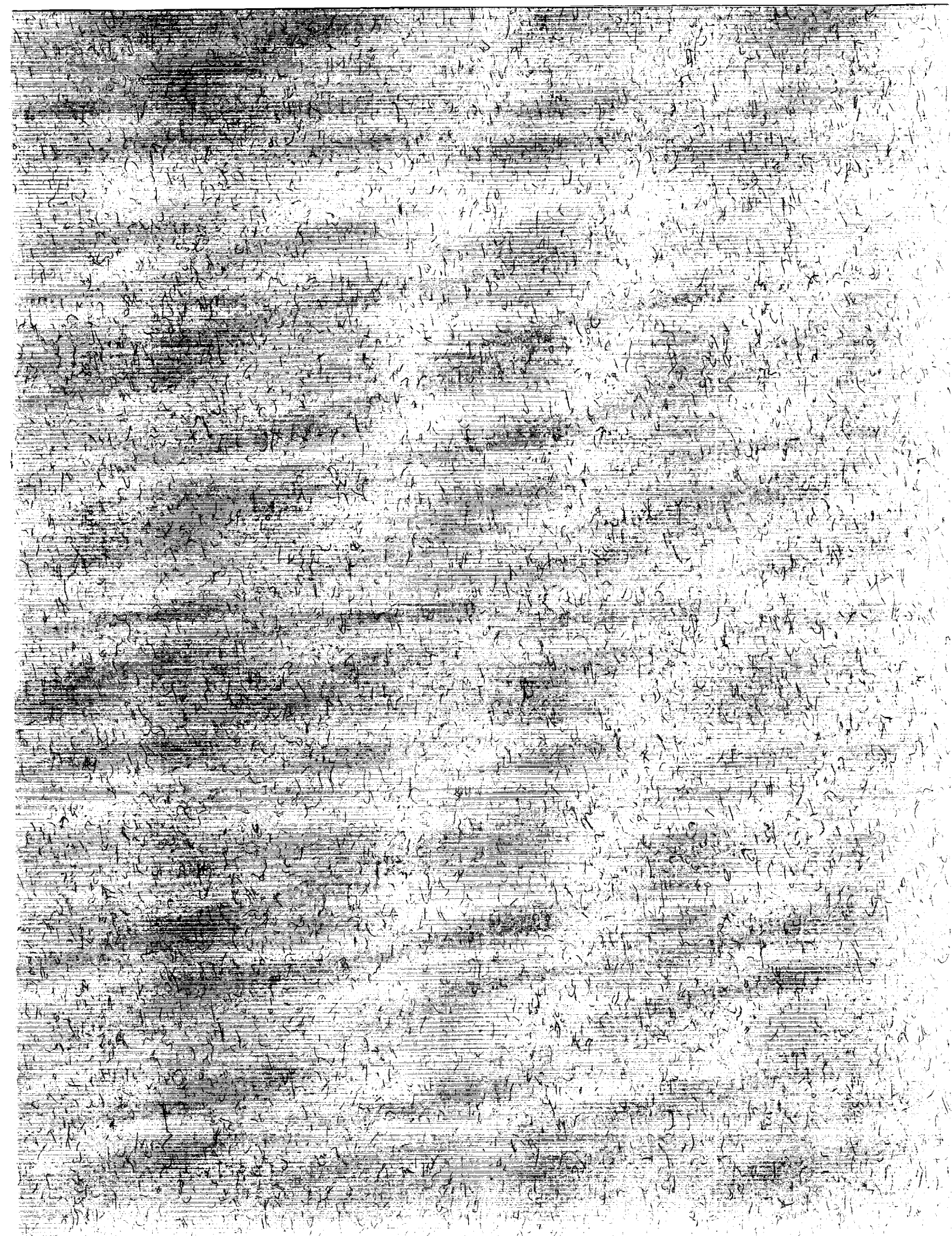




National Aeronautics and Space Administration

Report Documentation Page

1. Report No. NASA TP-2869		2. Government Accession No.		3. Recipient's Catalog No.	
4. Title and Subtitle Solar-Flare Shielding With Regolith at a Lunar-Base Site				5. Report Date December 1988	
				6. Performing Organization Code	
7. Author(s) John E. Nealy, John W. Wilson, and Lawrence W. Townsend				8. Performing Organization Report No. L-16488	
				10. Work Unit No. 506-49-31-01	
9. Performing Organization Name and Address NASA Langley Research Center Hampton, VA 23665-5225				11. Contract or Grant No.	
				13. Type of Report and Period Covered Technical Paper	
12. Sponsoring Agency Name and Address National Aeronautics and Space Administration Washington, DC 20546-0001				14. Sponsoring Agency Code	
15. Supplementary Notes					
16. Abstract The Langley Baryon Transport computer code BRYNTRN has been used to predict time-integrated radiation-dose levels at the lunar surface caused by high proton flux from solar flares. This study addresses the shielding requirements for candidate lunar habitat configurations necessary to protect crew members from large and unpredictable radiation fluxes. Three solar proton events have been analyzed, and variations in radiation intensity in a shield medium due to the various primary particle energy distributions are predicted. Radiation-dose predictions are made for various slab thicknesses of a lunar soil model. Results are also presented in the form of dose patterns within specific habitat configurations shielded with lunar material.					
17. Key Words (Suggested by Authors(s)) Lunar base Solar flares Radiation protection			18. Distribution Statement Unclassified—Unlimited		
			Subject Category 93		
19. Security Classif.(of this report) Unclassified		20. Security Classif.(of this page) Unclassified		21. No. of Pages 19	22. Price A02



National Aeronautics and
Space Administration
Code NTT-4

Washington, D.C.
20546-8801

Official Business
Penalty for Private Use, \$300

BULK RATE
POSTAGE & FEES PAID
NASA
Permit No. G-27

NASA

POSTMASTER: If Undeliverable (Section 118)
Postage Will Not Be Returned